Energy and exergy analysis of cold and power production from the geothermal reservoir of Torre Alfina

ENERGY AND EXERGY ANALYSIS OF COLD AND POWER PRODUCTION FROM THE GEOTHERMAL RESERVOIR OF TORRE ALFINA

Martina Leveni[1], Giampaolo Manfrida[2], Raffaello Cozzolino[1], Barbara Mendecka[2]

[1]Department of Industrial Engineering, University of Rome Niccolò Cusano, Via Don C. Gnocchi, 3 - 00016

[2]Department of Industrial Engineering - DIEF - University of Florence, Viale G. B. Morgagni, 40 - 44 - 50135

martina.leveni@unicusano.it, manfrida@unifi.it, raffaello.cozzolino@unicusano.it, barbara.mendecka@unifi.it

*****Corresponding author: martina.leveni@unicusano.it

Abstract

Geothermal power plants can provide clean and renewable energy and can be proposed as integrated units for simultaneous production of cooling and power. This paper presents a cascade arrangement of an organic Rankine cycle (ORC) and a water/lithium bromide (LiBr) absorption chiller (ABS). Starting from a literature reference layout which is taken as benchmark, some improvements are proposed at system level.

To assess the performance of the system, a thermodynamic model is developed in EES and the energy and exergy balance is calculated. The proposed system is re-evaluated with reference to resource conditions corresponding to a planned power plant in central Italy, Torre Alfina (TA). A sensitivity analysis is performed in order to investigate the operating range of the plant and the possibility of adapting its design to the requirements of the customers. Under optimized conditions, the TA Case (targeted on a 5 MW power output) showed an energy utilization factor (EUF) of 46.2% and an exergy efficiency of 27.7%, neglecting the brine reinjection loss. The highest exergy destructions occur in the ORC economizer (8.6%), in the ABS generator (6.3%) and absorber (5.5%). The good resource conditions in TA case drive the design optimization to production of power rather than cold.

Keywords: Geothermal Energy; Cold and Power Production; Organic Rankine Cycle; Absorption Cycle; Energy and Exergy analysis.

1 Introduction

The interest about renewable energy resources is rapidly growing as they represent a possible response to fulfill the increasing energy demand and reduce the environmental impact of fossil fuels and hence global warming [1].

Among the renewable energies, such as wind [2], solar [3], and hydroelectric [4], the geothermal energy is a promising alternative resource, which can be utilized for power generation, heating and cooling, or other production purposes [5].

Geothermal energy is a sustainable energy source with a low environmental impact, low greenhouse gas emissions and feasible technology [6], [7]. Moreover, unlike solar and wind energy, it is continuously available and independent of meteorological conditions [8], [9].

When the geothermal source has rather low temperatures (120-150 °C), binary power plants are considered as particularly appropriate [10], [11]. In such plants, the geothermal fluid does not directly produce power into the turbine, instead it is used to heat a low boiling point working fluid which then expands into the turbine [12], [13]. Typically the working fluid is an organic fluid, thus the Organic Rankine Cycle (ORC) is considered as one of the most attractive power cycles to extract thermal energy from low temperature geothermal sources [14], [15].The selection of the working fluid is a topic which is widely studied because it has a large influence on the performances of the cycle, as reported in [16], [17], [18].

Binary plants can be improved in terms of energy saving and resource economy when used for simultaneous generation of power and cooling, e.g. when the hot source is used not only to produce electricity, but also cold [19]. The research is very active regarding the design, development and optimization of combined production systems (also known as cogeneration systems) [20], [21] as well as in their operational planning, considering energy and economic issues [22], [23].

Recently, several low-enthalpy geothermal plants based on the organic Rankine cycle have been proposed for the combined production of different energy outputs.

Two different tri-generation systems, based on the organic Rankine cycle or Kalina cycle, coupled to a water/lithium bromide (LiBr) absorption chiller (ABS) and a water heater, are analyzed and compared in Zare [24]. The thermodynamic optimization showed that the

maximum exergy efficiency can reach values of 46.5% and 50.4% for the ORC and the Kalina cycle, respectively.

Tempesti et al. [21] presented two small size combined heat and power (CHP) systems based on the ORC in order to exploit at the same time a low-temperature geothermal resource (i.e. 90 °C) and solar energy. The performance of both configurations is calculated and compared for three different organic fluids: R134a, R236fa and R245fa. The best performance in terms of cycle energy and exergy efficiencies is obtained with the R245fa for both configurations; while the R134a proved to be attractive in terms of heat recovered at the de-super-heater (DSH) and the condenser.

Fiaschi et al. [25] proposed an innovative CHP system configuration called 'cross-parallel', as the ORC and the thermal utility circuits are set in parallel in order to improve the heat capacity matching. The system can provide heat at 80-140 °C which is suitable for industrial use, using a geo-fluid resource at slightly higher temperatures (130-170°C). The results demonstrate that at low temperature and low heat demand, the working fluids R227ea, R134a and R1234ze allow to obtain the greatest net power, while at high temperature and high heat demand, n-butane and R245fa are the most performing fluids. The optimized CHP system, compared to the traditional series configuration, shows an increase of the net electrical power output up to 55% for the investigated conditions, with a corresponding exergy efficiency of 70-78%.

Goswami at al. [26] proposed a combined power and cooling cycle using ammonia-water mixtures as a working fluid. Simulations show that the new cycle has a higher thermal efficiency compared to a conventional steam Rankine cycle operating between the same source and sink temperatures.

Fiaschi at al. [27] presented a combined cooling and power (CCP) system based on a water-ammonia power cycle enhanced with two refrigeration heat exchangers. The proposed cycle has an interesting potential of improving the electrical efficiency, compared to the traditional binary cycles, by using the heat source of the ORCs at a fixed temperature. The main advantage of this solution is the possibility of reducing the turbine outlet pressure, hence increasing the net power, the electrical efficiency and the second law efficiency to about 610 kW, 16.6% and 59.5% respectively. The CCP configuration also provides about 250 kW of cooling at temperature levels between 10°C and 15°C. The CCP configuration results in an economic

advantage, reducing the unit cost of electricity production from 0.22 $ / kWh of the basic power plant to about 0.18 $ / kWh.

Islam et al. [28] studied a hybrid solar-geothermal system based on two ORC power turbines, two thermal energy storage systems, an absorption chiller, a heat pump for space heating and a drying system. The results show energy and exergy efficiencies equal to 51% and 62% respectively, operating in multi-generation mode, whereas these efficiencies on single generation mode were in the order of 22% and 54%, respectively.

A geothermal CCP system, integrating a flash-binary system with a bottoming subsystem based on an organic Rankine cycle and an ejector refrigeration cycle, was proposed by Zhao et al. [29]. Parametric analyses and optimizations are performed. The effect on system performance of flash pressure, generator pinch point temperature difference, inlet pressure and back pressure of the turbine is evaluated. The results of the optimization show that the most effective system from the exergo-economic point of view may not obtain the best thermodynamic performance and vice versa.

Kordlar et al. [30] proposed a novel cogeneration system combining an organic Rankine cycle and an ammonia-water absorption refrigeration cycle fed by a geothermal resource. The results of the optimization of the three examined cases show that the total unit cost in case 3 (minimum total cost of the product unit) is about 20.4% lower than the corresponding value in case 1 (maximum efficiency of the first law) and about 24.3% lower than in case 2 (maximum efficiency of the second law). Moreover, case 3 presents a penalty of 10.21% decrease in the energy efficiency with respect to case 1 and a 4.5% reduction in the exergy efficiency with respect to case 2.

Several interesting studies on the production of cold and power are available in literature, but a comprehensive investigation of an actual geothermal site appears to be still missing.

In this paper, a plant based on an ORC coupled with a LiBr/water absorption chiller is tested on the real conditions of the geothermal reservoir of Torre Alfina (TA) in central Italy. The geothermal resource is first exploited by the ORC for the production of electricity, then the remaining energy content is used for cooling production in the ABS, as reported in Section 2.

Section 3 describes the thermodynamic modeling and presents the energy and exergy balances carried out to assess the performance of the plant. Furthermore, the Base Case with enhanced features with respect to the benchmark test case by Zare [24], is presented: in particular, the

sanitary water is suppressed, a preheater is added to the chiller and accurate working fluid properties are used for the simulation.

In Section 4, a preliminary verification of the Base Case against the benchmark case [24], is carried out. The model is then applied to the conditions of the TA reservoir (TA Case) with a target power output of 5 MW, according to the Italian law constraints [31]. The results and the conclusions are discussed, respectively, in Section 4 and 5.

In the context of a countryside area devoted to tourism and agriculture, the end-user of the cooling production could be hotel facilities as well as food processing industries, in particular for food conservation.

2 System description

The geothermal power and cooling plant here considered is based on the system proposed in [24]; a schematic is shown in Figure 1.

The plant is conceived as a cascade arrangement of the ORC on the top and the absorption cycle on the bottom: the geothermal brine first heats the ORC working fluid in the ORC heat exchanger (points 1-2). Then, the remaining sensible heat in the stream is exploited to feed the absorption cycle (points 2-3).

With respect to the layout proposed by [24], two main adjustments are performed. The large use of low-temperature heat for the sanitary water is suppressed. This choice is in practice justified by the necessity of reinjecting the brine with a limited temperature difference relatively to the resource conditions; moreover, it is very difficult to find local uses for extensive amounts of low-temperature heat.

A geothermal brine preheater (PH) was added upstream of the generator (GEN) of the absorption cycle, in order to effectively satisfy the physical condition that the reinjection temperature of the geothermal brine (T_3) has to be lower than the outlet temperatures of the generator (T_{18} and T_{33}) in the absorption cycle.

The ORC cycle is a saturated (Rankine) subcritical unit with dry (superheated) conditions at expander outlet; in order to simplify the layout no regenerative recovery of the de-super-heating is envisaged. The selected working fluid of the ORC is isobutane. Dry and isentropic fluids are more suitable for the ORC operation thanks to the superheated condition after the expansion

process [32]. Moreover, the working fluid should satisfy safety criteria and have a reduced environmental impact. The properties of isobutane best match all these characteristics [33]. In fact, isobutane is extensively used in the ORC systems for power generation from geothermal resources [34], [35].

Regarding the absorption cycle, the evaporator (EVA) provides the cooling load, which is represented by the cooled stream (points 23-24) while the regenerative heat exchanger provides effective heat recovery between the rich (points 18-19) and poor (points 16-17) solution streams. The choice of a water/LiBr absorption chiller is based on the targeted refrigeration temperature of 8°C (point 24) [36].

The vapor exits the generator of the absorption cycle (point 11) at the saturation temperature of the entering solution stream (point 33) [37].

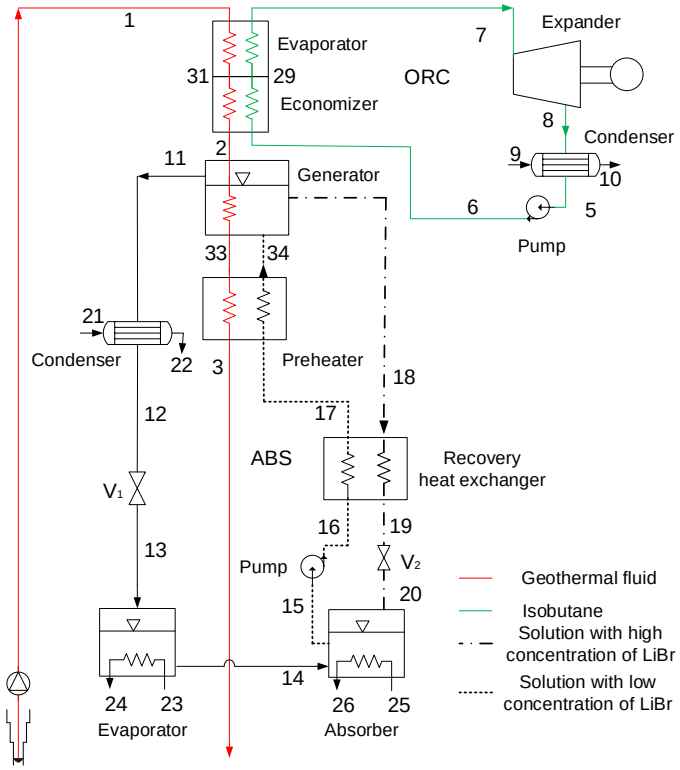

Figure 1: Geothermal power and cooling plant - Schematic

3 System modeling

In this section the numerical model of the system, including the organic Rankine cycle and the LiBr/water absorption chiller, is presented.
The model is based on the following assumptions:

- the system is simulated under steady-state condition;
- the refrigerant at the outlet of the condenser (CD_{ABS}) is saturated liquid;
- the refrigerant at the outlet of the evaporator (EVA_{ABS}) is saturated vapor;
- the expanding process in the throttling valves is isenthalpic;
- the turbine and pump are operated with assigned values of isentropic efficiencies;
- the pressure drops in the pipelines and in the heat exchangers are neglected;
- changes in kinetic and potential energies are neglected.

3.1 Energy analysis

In order to perform the energy analysis of the system, the principles of mass conservation and first law of the thermodynamic are applied to each component, resulting in a system of equations representing the plant model.

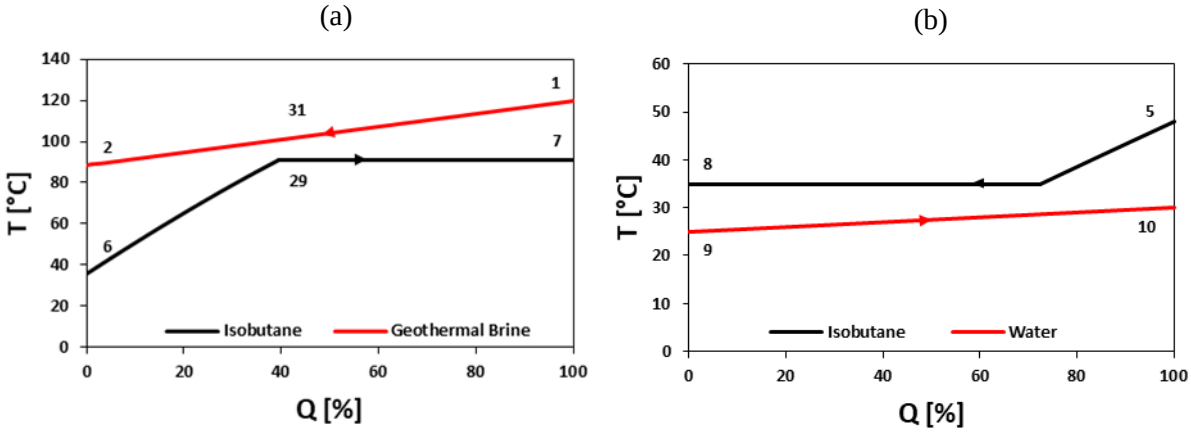

Figure 2: ORC pinch diagrams: (a) Heat exchanger (HE_{ORC}) (b) Condenser (CD_{ORC})

The temperature-heat curves of the evaporator and economizer of the ORC are shown in Figure 2a, while Figure 2b presents the same profiles for the condenser of the ORC. With reference to this Figure, the energy balance of the evaporator can be written in order to calculate the mass flow rate of the ORC working fluid:

$$\dot{Q}_{ORC,EVA} = \dot{m}_{GB}(h_1 - h_{31}) = \dot{m}_{ORC}(h_7 - h_{29}) \quad (1)$$

With:

$$\Delta T_{P,ORC} = T_{31} - T_{29} \quad (2)$$

Where T_{29} is the outlet temperature of the working fluid at the economizer and T_{31} is the inlet temperature of the geothermal fluid at the economizer. The difference between these points corresponds to the pinch point as defined in Eq. 2.
The energy balance of the economizer section allows to calculate T_2:

$$\dot{Q}_{ORC,ECO} = \dot{m}_{GB}(h_{31} - h_2) = \dot{m}_{ORC}(h_{29} - h_6) \quad (3)$$

Conditions at point 6 are determined from the energy balance of the condenser and from the power of the pump (calculated from the ideal performance by using the isentropic efficiency):

$$\dot{Q}_{ORC,CD} = \dot{m}_{ORC}(h_8 - h_5) = \dot{m}_{CW}(h_{10} - h_9) \quad (4)$$

$$h_6 = h_5 + \dot{W}_{ORC,PUMP}/\dot{m}_{ORC} \quad (5)$$

The power output from the turbine is given by:

$$\dot{W}_{ORC,EXP} = \dot{m}_{ORC}(h_7 - h_8) = \dot{m}_{ORC}\eta_{ORC,EXP}(h_7 - h_{8s}) \quad (6)$$

The power input to the pump is given by:

$$\dot{W}_{ORC,PUMP} = \dot{m}_{ORC}(h_6 - h_5) = \dot{m}_{ORC}\frac{(h_{6s} - h_5)}{\eta_{ORC,PUMP}} \quad (7)$$

The first law efficiency of the ORC cycle is eventually calculated as:

$$\eta_{ORC} = \frac{\dot{W}_{ORC,EXP} - \dot{W}_{ORC,PUMP}}{\dot{Q}_{ORC,EVA} + \dot{Q}_{ORC,ECO}} \quad (8)$$

Regarding the absorption cycle, the analysis starts with the GEN energy balance:

$$\dot{Q}_{ABS,GEN} = \dot{m}_{GB}(h_2 - h_{33}) = \dot{m}_{11}h_{11} + \dot{m}_{18}h_{18} + \dot{m}_{33}h_{33} - \dot{m}_{34}h_{34} \quad (9)$$

$$\dot{Q}_{ABS,PH} = \dot{m}_{GB}(h_{33} - h_3) = \dot{m}_{34}(h_{34} - h_{17}) \quad (10)$$

In Eqs. 8 and 9, it is assumed that $T_{33} = T_{18}$ (bulk liquid temperature at GEN), and $T_{34} = T_{18} - \Delta T_{a,GEN}$. The energy balance of the recovery heat exchanger (RHE) is written:

$$\dot{Q}_{ABS,RHE} = \dot{m}_{17}(h_{17} - h_{16}) = \dot{m}_{18}(h_{18} - h_{19}) \quad (11)$$

With $\dot{m}_{17} = \dot{m}_{34}$. The analysis of the cycle proceeds with the energy balances of the absorber (AB) and of the condenser (CD):

$$\dot{Q}_{ABS,AB} = \dot{m}_{25}(h_{26} - h_{25}) = \dot{m}_{20}h_{20} + \dot{m}_{14}h_{14} - \dot{m}_{15}h_{15} \quad (12)$$

$$\dot{Q}_{ABS,CD} = \dot{m}_{11}(h_{11} - h_{12}) = \dot{m}_{21}(h_{22} - h_{21}) \quad (13)$$

With $\dot{m}_{15} = \dot{m}_{17}$; $\dot{m}_{20} = \dot{m}_{18}$; $\dot{m}_{14} = \dot{m}_{11}$. Note that $h_{13} = h_{12}$ and $h_{20} = h_{19}$ because the laminar valve expansion is assumed as an isenthalpic process.

As for the ORC, the pump performance determines the value of h_{16}:

$$h_{16} = h_{15} + \dot{W}_{ABS,PUMP}/\dot{m}_{15} \quad (14)$$

Finally, the useful cold output of the absorption cycle is:

$$\dot{Q}_{ABS,EVA} = \dot{m}_{24}(h_{23} - h_{24}) = \dot{m}_{14}(h_{14} - h_{13}) \quad (15)$$

The set of Eqs. 9-15, with the necessary input data, determines all the variables needed to solve the problem and calculate the output of the absorption cycle, which is resumed by its coefficient of performance (COP):

$$\mathrm{COP}_{ABS} = \frac{\dot{Q}_{ABS,EVA}}{\dot{Q}_{ABS,GEN} + \dot{Q}_{ABS,PH}} \quad (16)$$

Note that the work of the pump in the ABS is neglected when calculating the coefficient of performance, as it presents a very small contribution and can be considered as a system auxiliary.

To evaluate the overall performance of the co-generative system considered in the present work, the Energy Utilization Factor (EUF), as reported in [24], is expressed as follows:

$$\mathrm{EUF} = \frac{\dot{Q}_{ABS,EVA} + \dot{W}_{ORC,EXP}}{\dot{Q}_{in}} = \frac{\dot{Q}_{ABS,EVA} + \dot{W}_{ORC,EXP}}{\dot{m}_{GB}(h_1 - h_3)} \quad (17)$$

The logarithmic mean temperature difference method (LTMD) is used to evaluate the area of the heat exchangers. The LMTD is defined by the logarithmic mean as follows:

$$\mathrm{LMTD} = \frac{\Delta T_A + \Delta T_B}{ln\frac{\Delta T_A}{\Delta T_B}} \quad (18)$$

Where ΔT_A is the temperature difference between the two streams at the hot side and ΔT_B is the temperature difference between the two streams at the cold side. Finally, the LMTD is used to

find the area of the heat exchangers.

$$\mathrm{A} = \frac{\dot{Q}}{U \cdot LMTD} \tag{19}$$

Where U is the overall heat transfer coefficient.

3.2 Exergy analysis

The exergy analysis allows the evaluation of an efficiency index which is based on the fraction of the energy input that is actually convertible and on the distribution of irreversibilities (exergy destructions and losses) among the system components [38],[39]. The exergy approach is particularly useful when dealing with multipurpose systems (power and cold in this case). Moreover, the reconstruction of the full exergy balance at a component level can be used to calculate and check the exergy efficiency both in direct and indirect mode, thus validating the results and allowing the identification of the major irreversibilities.

The total exergy flow is calculated for each thermodynamic state as follows:

$$Ex_t = \dot{m} \cdot [(h - h_0) - T_0 \cdot (s - s_0)] = \dot{m} \cdot ex \tag{20}$$

The exergy destruction and/or exergy loss can be evaluated for each component as:

$$Ex_D = Ex_{t_{in}} - Ex_{t_{out}} \tag{21}$$

and

$$Ex_L = Ex_{t_{out,env}} \tag{22}$$

The exergy efficiency of the whole system is defined as the ratio of the exergy of the output products (cold and power) to the input exergy:

$$\eta_{xd} = \frac{\dot{W} + \left(\dot{E}x_{t_{24}} - \dot{E}x_{t_{23}}\right)}{\dot{E}x_{t_{in}}} \tag{23}$$

where the inlet exergy is considered as $\dot{E}x_{t_{in}} = \dot{E}x_{t_1}$(in the general case, it is assumed that the geothermal resource can be brought to full thermo-mechanical equilibrium with the environment).

An indirect validation of Eq. 23 can be performed considering exergy destructions and losses in all components:

$$\eta_{xi} = 1 - \frac{\sum_i \dot{E}x_{D_i} + \sum_j \dot{E}x_{L_j}}{\dot{E}x_{t_{in}}} \tag{24}$$

3.3 Base case and Italian Geothermal site case (Torre Alfina case)

The proposed system appears to be adaptable to different resource conditions. Then, the layout presented in Figure 1 and described in Section 2 is applied to two different cases, the first one, called "Base Case", refers to the source conditions retrieved from Zare [24]; the second case refers to the real conditions of the geothermal resource of Torre Alfina and is called "TA case'. Torre Alfina (TA) is considered, because it is a geothermal site under current development offering extensive documented results on well productivity and resource conditions; these data are available on the website of the Italian Ministry of Economic Development [40], [40] and on the Environmental Impact Assessment documentation available on the public web repository of the Ministry for the Environment and Protection of the Land and Sea [41].

In Italy, the Legislative Decree n. 22 issued in February 2011 provides that, in order to promote research and development of new geothermal power plants with reduced environmental impact, fluids with medium and high enthalpy are considered of national interest. The national regulatory guidelines for special permits point to advanced-technology plants with geothermal fluids reinjection in the same original formations with the absence of emissions in the atmosphere and with a nominal installed power not exceeding 5MWe for each plant. The present study focuses on the Castel Giorgio-Torre Alfina site, a mining concession directed to experimental pilot plant (UNMIG) shown in Figure 3. The site is located between Lazio and Umbria regions, in Central Italy close to Bolsena Lake.

At the reservoir top, at a depth of about 550 m, a CO_2 gas cap with a pressure of about 45 bar has been found in the central part of the field. Under the gas cap, there is the aquifer with a

uniform temperature of about 140°C, due to the presence of a strong convective circulation, and a content of CO2 of about 2% [42], [43].

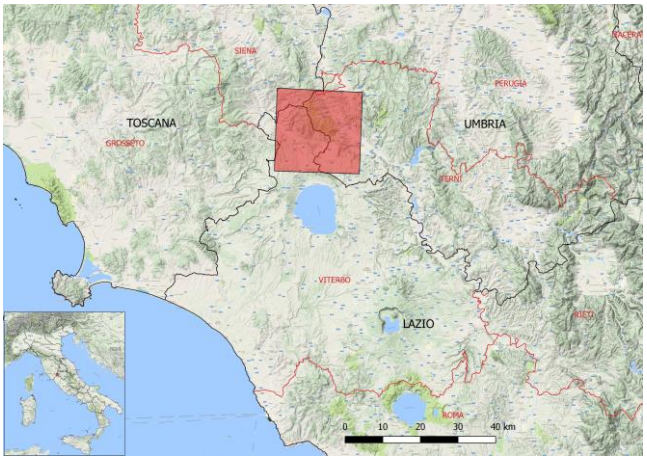

Figure 3: Torre Alfina mining concession

The operating parameters for the Base and TA Cases are taken from [24], [40], [40], [41], and are summarized in Table 1. The Base Case assumes an ORC expander inlet temperature of T_7 = 90°C as reported in [24]. In the TA Case a power output $\dot{W}_{ORC,EXP}$ = 5 MW is assumed according to [31]; an upper cycle pressure of p_7 = 3158 kPa is selected, resulting from an optimization process performed using isobutane as working fluid. T_3 and T_7 are calculated from the energy balance at the preheater and the evaporator, respectively.

Table 1- Systems operating parameters

	Base Case [24]	**Torre Alfina Case** [40],[40],[41]
Parameter	**Value**	**Value**
p_0 [kPa]	101.325	101.325
T_0, T_9 [°C]	25	25
T_{GB}[°C]	120	140
p_{GB} [kPa]	208.5	4400
$\dot{m}_{GB}$ [kg/s]	100	292
η_T, η_P [-]	0.85	0.85
ΔT_{PP} [°C]	10	4.4

$Range_{ORC}$ [°C]	5	5
DTU_{CD} [°C]	5	5
$Range_{ABS,CD}$ [°C]	10	10
$Range_{ABS,AB}$ [°C]	8	8
T_{15} [°C]	36	36
T_{12} [°C]	35	35
T_{18} [°C]	77	85
T_{14} [°C]	5	5
$\Delta T_{a,EVAC}$ [°C]	8	8
$\Delta T_{a,EVAH}$ [°C]	3	3

To assess the performance of the proposed power and cooling system, for the Base and Italian site Cases, the model is implemented in the Engineering Equation Solver (EES) software, a general equation-solving program with access to highly accurarate thermodynamic property databases [44].

It is important to highlight that, to build the Base Case, some adjustments are performed with respect to the layout and the data provided in the work by Zare [24]. This is necessary because of the following reasons:

a) Data provided in [24] are not accurate; specifically, at p_7 = 15 bar, accurate iso-butane property data state that the vapor saturation temperature is T_7 = 90°C. The updated data are reported in Table 2 and are consistent with values taken from the NIST (National Institute of Standards and Technology) website.
b) Pinch conditions should be respected in the GEN of the ABS cycle; that is, the temperature of the cooled geothermal brine at the absorber generator outlet must be lower than the temperature of the outgoing LiBr solution (18 rich solution). In order to respect this thermal pinch condition, it was necessary to include a preheater PH, introducing an intermediate point 33 (geothermal brine after PH and before GEN) with T_{33}=T_{18}. The present model includes a check of negative pinches along all heat transfer processes in the heat exchangers network. Such feature resulted to be very useful when

running parametric analyses and examining the performance sensitivity to the design parameters.

c) A new, more accurate set of equations of state (the external library LiBrSSC.DLL available for EES) is used for aqueous lithium bromide mixture [37], which leads to minor adjustments in the calculated thermodynamic variables for the absorption circuit.

4 Results and discussion

4.1 Validation

In this section, the model verification against the work of Zare [24] is presented. The calculated results obtained with the model applied to the Base Case show good accordance with those reported in [24], as summarized in Table 2. The calculated thermal efficiency of the ORC is equal to 10.4% and the coefficient of performance (COP) of the ABS is 0.85.

Table 2 - Operating conditions: (a) Base Case (b) Ref. [24]

Points	**p**		**T**		**ṁ**		**h**	**s**	**e**	**Ex**
-	*kPa*		*°C*		*kg/s*		*kJ/kg*	*kJ/kgK*	*kJ/kg*	*kW*
Geothermal Brine										
	a	b	a	b	a	b	a	a	a	a
1	208.5	208.5	120.0	120.0	100.0	100.0	503.8	1.5	52.8	5284.0
2	208.5	208.5	87.2	88.9	100.0	100.0	365.4	1.2	24.0	2401.0
3	208.5	208.5	76.9	80.0	100.0	100.0	321.9	1.0	17.0	1704.0
Organic Rankine Cycle										
5	464.5	402.4	35.0	34.8	36.3	32.2	284.3	1.3	50.7	1838.0
6	1640.0	1509.0	35.8	35.0	36.3	32.2	286.9	1.3	52.9	1918.0
7	1640.0	1509.0	90.0	90.1	36.3	32.2	668.6	2.4	111.4	4041.0
8	464.5	402.4	47.9	43.9	36.3	32.2	626.4	2.4	62.2	2258.0
9	101.3	100.0	25.0	25.0	593.6	562.0	104.9	0.4	0.0	0.0
10	101.3	100.0	30.0	30.1	593.6	562.0	125.8	0.4	0.2	102.9
29	1640.0	-	90.0	-	36.3	-	435.5	1.7	69.7	2528.0
31	208.5	-	100.0	-	100.0	-	419.2	1.3	34.1	3409.0
Absorption Cycle										
11	5.6	5.6	70.1	80.1	1.6	1.9	2631.0	8.6	84.6	131.7
12	5.6	5.6	35.0	35.1	1.6	1.9	146.6	0.5	0.6	0.9
13	0.9	0.9	5.0	5.1	1.6	1.9	146.6	0.5	-6.2	-9.6
14	0.9	0.9	5.0	5.1	1.6	1.9	2510.0	9.0	-176.1	-274.0
15	0.9	0.9	36.0	35.1	27.9	22.4	92.7	0.2	30.7	858.8
16	5.6	5.6	36.0	35.1	27.9	22.4	92.7	0.2	30.7	858.8
17	5.6	5.6	72.5	62.2	27.9	22.4	167.6	0.5	38.1	1064.0
18	5.6	5.6	77.0	62.2	26.4	20.5	186.9	0.5	57.7	1522.0
19	5.6	5.6	36.6	48.6	26.4	20.5	107.6	0.2	49.4	1302.0
20	0.9	0.9	36.6	48.6	26.4	20.5	107.6	0.2	49.4	1302.0
21	101.3	100.0	25.0	25.0	92.5	111.1	104.9	0.4	0.0	0.0
22	101.3	100.0	35.0	35.1	92.5	111.1	146.7	0.5	0.7	63.4
23	101.3	100.0	13.0	13.1	175.3	209.6	54.7	0.2	1.0	182.2
24	101.3	100.0	8.0	8.0	175.3	209.6	33.7	0.1	2.1	370.3
25	101.3	100.0	25.0	25.0	124.2	132.3	104.9	0.4	0.0	0.0
26	101.3	100.0	33.0	35.1	124.2	132.3	138.4	0.5	0.4	54.8
33	208.5	-	77.0	-	100.0	-	322.6	1.0	17.1	1713.0
34	5.6	-	74.0	-	27.9	-	169.8	0.5	37.7	1054.0

To further prove the reliability of the model, a parametric analysis with variable ORC turbine inlet temperature is also performed, as it is done in the reference: the results are compared in Figure 4. It can be noted that the range of the possible inlet operating temperatures is different

(82-96 °C in the present calculations, while the range of the analysis in [24] is 80-105°C). In fact, it has been observed that if T_7 = 96 °C is exceeded, the heat exchanged in the preheater becomes negative, which is not physically possible. This is the reason that raised the necessity of adding a preheater in the final layout, which allows to avoid negative pinch conditions.

On the one hand, the results in Figure 4 demonstrate a good match between the present model and [24] regarding the electrical power data. On the other hand, the cooling power results to be lower, although it shows the same trend of the literature data [24]. This is mainly due to the lower value of T_{11} = 70.1°C for the Base Case (saturated conditions, following [37]; in [24] a value of 80°C was assumed).

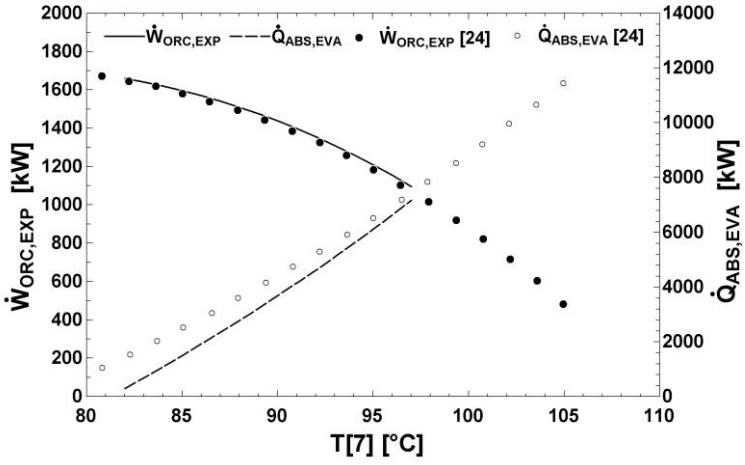

Figure 4: Validation of the Base Case on Ref. [24]

4.2 Sensitivity analysis

In order to determine the operating range and the possibility of adapting the plant design to possible requirements of the customers (interested to a dual-purpose plant, producing electricity and cold), several parametric analyses were carried out for the Torre Alfina (TA) Case.

The first parametric analysis is directed to assess the correct design conditions for the ORC section. The thermodynamic efficiency of the ORC and the efficiency of the ORC heat exchanger (ECO+EVA) are calculated as a function of the high pressure of the cycle. The product of these two efficiencies results in the overall efficiency of the cycle. Figure 5 shows that isobutane tends to optimize the performance for pressure conditions (p_7 = 3158 kPa) close

to critical. This value is consequently selected as a design pressure for the TA site. By imposing that the power must not exceed the maximum power of 5 MWe (constrained by the concession rules), the value of T_3 = 83.7°C is determined, which is consistent with reinjection conditions into the geothermal reservoir that prevent scaling issues and guarantee long-term operation of the reservoir.

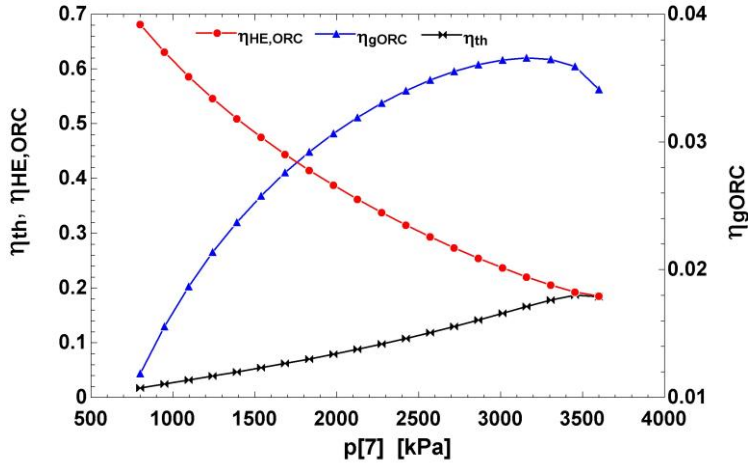

Figure 5: Effect on ORC performance parameters of the turbine inlet pressure

From the economic point of view, the cost of the heat exchanger, that is directly related to the extension of their surface area, represents the main investment cost for a geothermal ORC system. In principle, a decrease of ΔT_{PP} determines an improvement in performance, but is paid in terms of increased heat transfer surface [45]. With the constraints here applied on the geo-fluid temperature profile, one may consider working in conditions of non-optimal performance: lower values of p_7 (only subcritical ORC cycles are here considered) determine larger ΔT_{PP}, which in turn affect the heat transfer surface. For this reason, a parametric analysis is performed to evaluate how variations in p_7 affect the ΔT_{PP} in the high pressure heat exchanger of the ORC (HE_{ORC}), and consequently the influence on the temperature profiles and the performance of the system as well as the heat exchanger surface area. The analysis is performed keeping the brine mass flow rate and the inlet temperature of the resource T_1 at constant values, while the desired net power is fixed at 5 MW. The results of the analysis are shown in Figure 6.

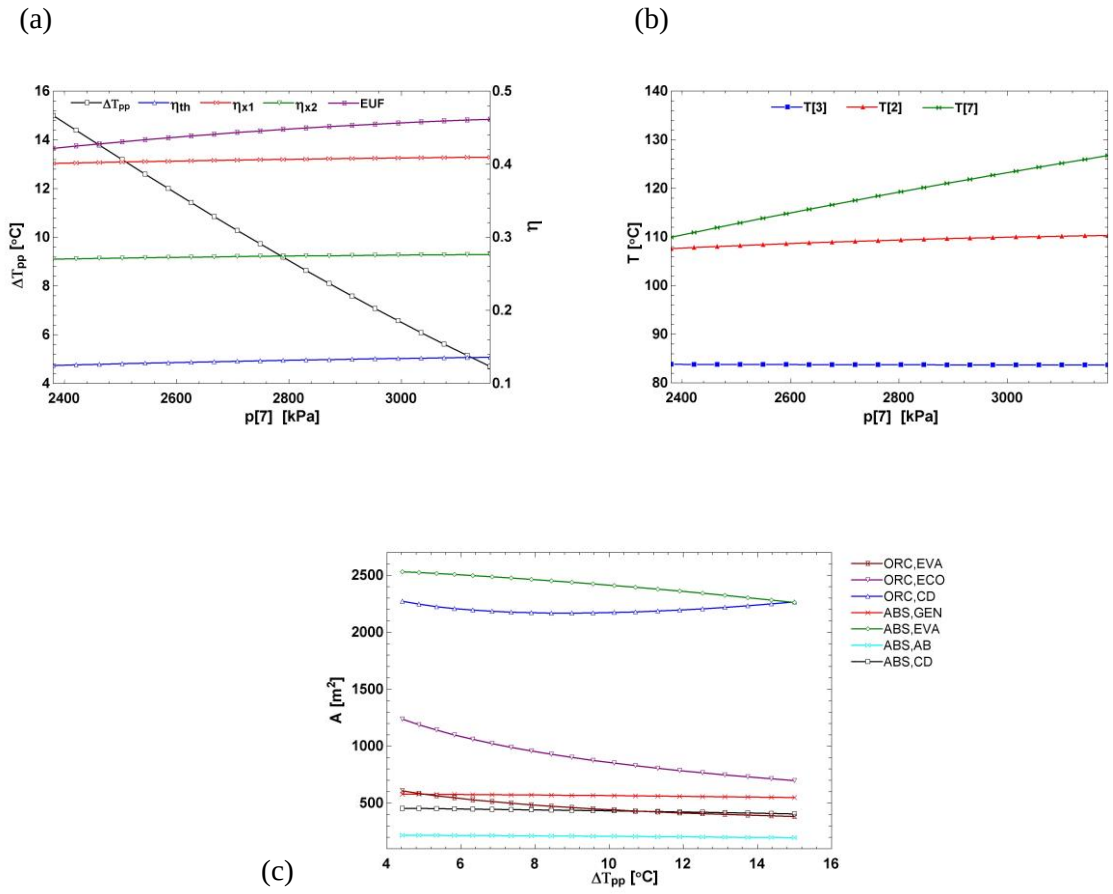

Figure 6: Influence of pinch point temperature difference on system performances

Figure 6a shows on the right side scale the thermodynamic efficiency, the energy utilization factor (EUF) and of the exergy efficiencies η_{x1} and η_{x2} (this last including the brine reinjection loss) as a function of p_7. The same picture shows on the left side scale that there is an approximately linear dependence of ΔT_{PP} on p_7, with a variation of ΔT_{PP} from about 4°C to 15°C in the range of p_7 here considered.

The thermodynamic efficiency η_{th} increases as the pressure is increased and the ΔT_{PP} is decreased. Moderate variation of the exergy efficiencies is observed, with a positive trend as the turbine inlet pressure is increased and the ΔT_{PP} is decreased. The EUF increases as the pressure is increased and the ΔT_{PP} is decreased.

The effect of a variation in the value of ΔT_{PP} on the relevant temperatures is shown in Figure 6b. The evaporation temperature T_7 decreases with the increasing ΔT_{PP}, if $\dot{W}_{ORC,EXP}$ and the geothermal brine temperature are kept constant. Higher ΔT_{PP} allows for a slightly decreased geothermal brine outlet temperature T_2, i.e. from 110.3°C to 107.6°C. On the other hand, the reinjection temperature T_3 shows variation of less than 1°C over the whole range of p_7 and ΔT_{PP}. The influence of ΔT_{PP} on the surfaces of all the heat exchangers of the system is shown in Figure 6c. Values of the overall heat transfer coefficient between 848 W/m^{2}K and 3134 W/m^{2}K are applied, following [46] and [47]. Figure 6c shows that the surfaces of the absorber, of the condenser and of the generator in the ABS are relatively insensible to changes in p_7.

As expected, the area of the economizer and evaporator of the ORC decrease, as the ΔT_{PP} increases, from 1238 m^2 to 699 m^2 and from 2532 m^2 to 2261 m^2 respectively. The condenser in the ORC presents a slight sensitivity to ΔT_{PP}, reaching a minimum surface of 2168 m^2 for a ΔT_{PP} = 9°C. It is worth noting that the cooling to power ratio decreases from 5.42 to 4.84 as the ΔT_{PP} decreases. This is due to the reduced value of the evaporator temperature T_2 as shown in Figure 6b. The previous parametric analysis based on the ORC high pressure (Figure 5) suggests an optimal value of p_7 = 3158 kPa, which implies a HE_{ORC} pinch point temperature difference of 4.4°C. This does not result in dramatic consequences in terms of heat transfer surface, and is thus taken as the reference design condition for the TA Case.

A final parametric analysis is directed to demonstrate the possible flexibility of the design. Maximizing the thermal efficiency of the ORC section is not necessarily corresponding to the customer's needs for a dual-purpose plant. Power and cold are both valuable products, whose relative importance is very sensitive to the ORC working fluid mass flow rate. For this sensitivity analysis, the geothermal brine mass flow rate and the temperature T_1 of the resource were constant; the ΔT_{PP} for the HE_{ORC} component is kept fixed to the optimal value of 4.4 °C, obtained by adjusting the inlet turbine pressure p_7.

Figure 7a shows that as the organic fluid flow rate $\dot{m}_{WF}$ is increased from 50 kg/s to 120 kg/s, the electric power output increases from 2575 kW to 6367 kW. On the other hand, for the same increase of $\dot{m}_{WF}$, the cooling power decreases sharply, from 42672 kW to 17602 kW, since the temperature of Point 2 (and consequently the input thermal power to GEN) is reduced. Thus, the power to cooling ratio obtained varies from 0.06 to 0.36. It is therefore possible to cover

with an *ad hoc* management different necessities of the customer in terms of power and cold production.

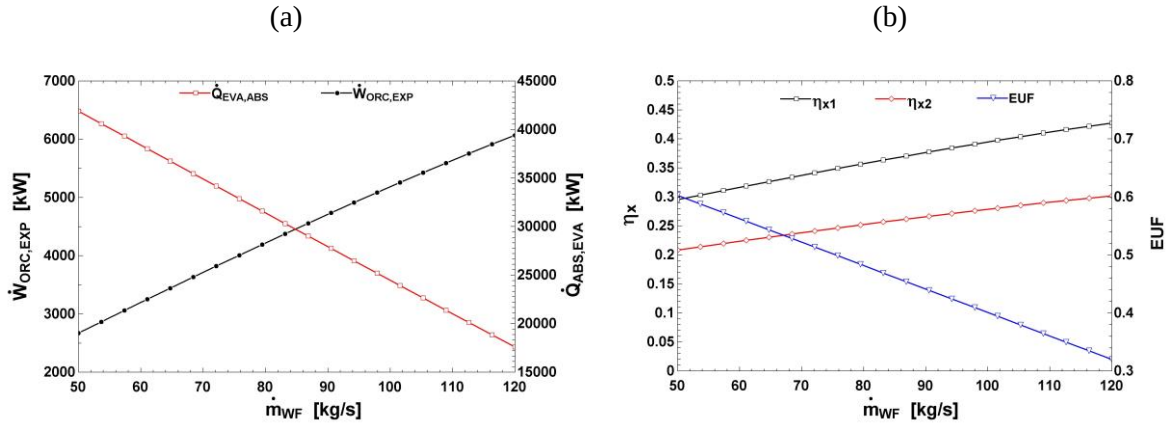

Figure 7: Influence of the working fluid mass flow rate on system performance

Figure 7b shows the variation of the exergy efficiencies η_{x1} (which neglects the reinjection loss), η_{x2} (including the reinjection loss) and the Energy Utilization Factor EUF. Both global exergy efficiencies increase as the working fluid mass flow rate is augmented. This is mainly due to the increase in $\dot{W}_{ORC,EXP}$, an exergy output contribution which is much larger than the decrease in the cold exergy output $\left(\dot{E}x_{t_{24}} - \dot{E}x_{t_{23}}\right)$ (Eq. 23). As for the EUF, an increase in the working fluid mass flow rate results in a decrease of this performance parameter. The main logical reason behind this is that an increase in the working fluid mass flow rate decreases the production of cold.

The parametric analysis carried out can be a useful tool for the control of the system, as it demonstrates the possibility to adapt the amount and quality of the two energy products (electricity and cold) depending on the customer requirements.

4.3 Energy and exergy analysis

Table 3 lists the significant thermodynamic properties, mass flow rates and exergy at each point of the proposed system for the TA Case. The thermal efficiency of the ORC for the TA site is

equal to 13.6%. The coefficient of performance (COP) of the ABS cycle is 0.83. Considering the whole system for TA site, the EUF is 46.2%.

Table 3- Calculated properties at the geothermal plant for Torre Alfina site

Points	**p**	**T**	**ṁ**	**h**	**s**	**e**	**Ex**
-	*kPa*	*°C*	*kg/s*	*kJ/kg*	*kJ/kgK*	*kJ/kg*	*kW*
Geothermal Brine							
1	4400.00	140.0	292.00	591.80	1.7350	79.00	23082
2	4400.00	110.3	292.00	465.70	1.4185	47.40	13839
3	4400.00	83.7	292.00	354.00	1.1163	25.70	7500
Organic Rankine Cycle							
5	464.50	35.0	93.38	284.30	1.2883	50.70	4731
6	3158.00	36.87	93.38	290.20	1.2911	55.70	5201
7	3158.00	126.3	93.38	684.30	2.3591	131.40	12271
8	464.50	47.11	93.38	624.90	2.3922	62.10	5803
9	101.30	25.0	1522.00	104.90	0.3672	0.00	0.03815
10	101.30	30.0	1522.00	125.80	0.4367	0.20	263.8
29	3158.00	126.3	93.38	564	2.0578	100.9	9423
31	4400.00	131	1522.00	553.3	1.6408	68.6	20043
Absorption Cycle							
11	5.63	70.1	11.45	2631.00	8.5569	84.60	968.8
12	5.63	35.0	11.45	146.60	0.5051	0.60	6.751
13	0.87	5.0	11.45	146.60	0.5279	-6.20	-70.82
14	0.87	5.0	11.45	2510.00	9.0249	-176.10	-2016
15	0.87	36.0	106.30	92.66	0.2245	30.70	3268
16	5.63	36.0	106.30	92.66	0.2245	30.70	3268
17	5.63	74.3	106.30	171.30	0.4616	38.70	4110
18	5.63	85.0	94.87	218.50	0.4693	83.60	7932
19	5.63	38.06	94.87	130.40	0.2082	73.40	6959
20	0.87	38.06	94.87	130.40	0.2082	73.40	6959
21	101.30	25.0	680.40	104.90	0.3672	0.00	0
22	101.30	35.0	680.40	146.70	0.5051	0.70	466.5
23	101.30	13.0	1290.00	54.70	0.1953	1.00	1340
24	101.30	8.0	1290.00	33.73	0.1213	2.10	2724
25	101.30	25.0	934.60	104.90	0.3672	0.00	0
26	101.30	33.0	934.60	138.40	0.4779	0.40	411.9

33	4400.00	85.0	292.00	359.40	1.1316	26.60	7765
34	5.63	82.0	106.30	186.30	0.5067	40.20	4276

Finally, Figure 8 presents the T-s diagrams for the Base Case and for TA Case. Figure 8b shows that the expansion line, assumed as a straight line, crosses the two-phase region. However, as reported in [48] if the working fluid enters and exits the dome in the vapor phase, droplets do not have time for formation. Moreover, in this case the quality is always higher than 0.96. Gyarmathy [49] shows that Wilson nucleation point typically occurs when 3.5-5% moisture is present and Besarati et al. [50] observe that a quality of 0.9 did not have any effect on the expander efficiency. In conclusion, given the high values of the quality during the expansion, there are no concerns about the safe operation of the turbine.

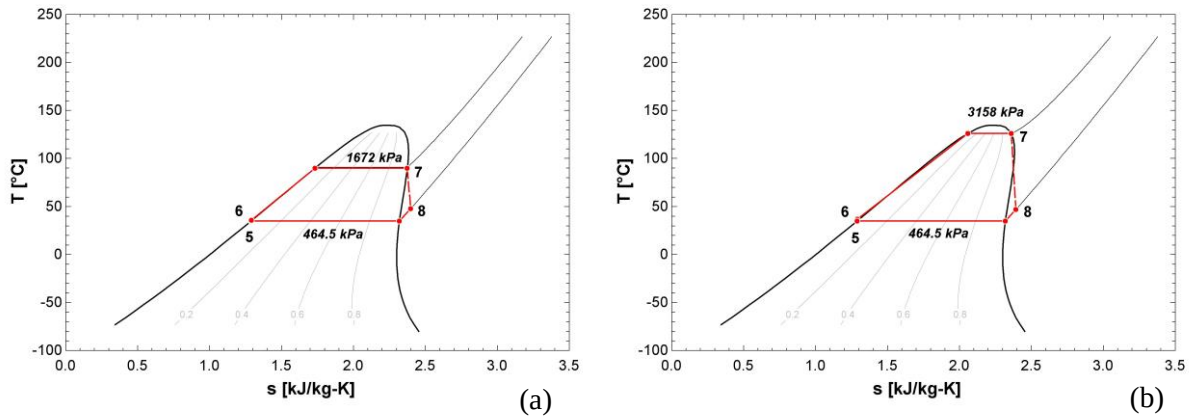

Figure 8: ORC T-s chart: (a) Base Case (b) Torre Alfina Case

The exergy analysis is summarized in Figure 9, collecting data on relative exergy destructions and losses (made non-dimensional with respect to the inlet exergy $\dot{E}x_{t_1}$). A reference ambient temperature of 298.15 K is assumed.

Regarding the Base Case, the brine reinjection loss (47.6%) is considered separately since a relatively high reinjection temperature (T_3 = 76.9 °C) is retained, as is common practice in order to avoid perturbation of the reservoir heat balance. The exergy efficiency when the reinjection losses are neglected ($\dot{E}x_{t_{in}} = \left(\dot{E}x_{t_1} - \dot{E}x_{t_3}\right)$) is equal to η_{x1} = 0.4542. If the brine reinjection loss is considered, the exergy efficiency (Eqs. 22 and 23) is equal to η_{x2} = 0.308.

The objective of the exergy analysis, in the case of a geothermal plant, is to identify the components responsible of the highest exergy destruction or loss. As is shown in Figure 9, these can occur in the ORC economizer (7.5%) and evaporator (6.8%), while the ABS components have relatively low exergy destructions (below 2.5%).

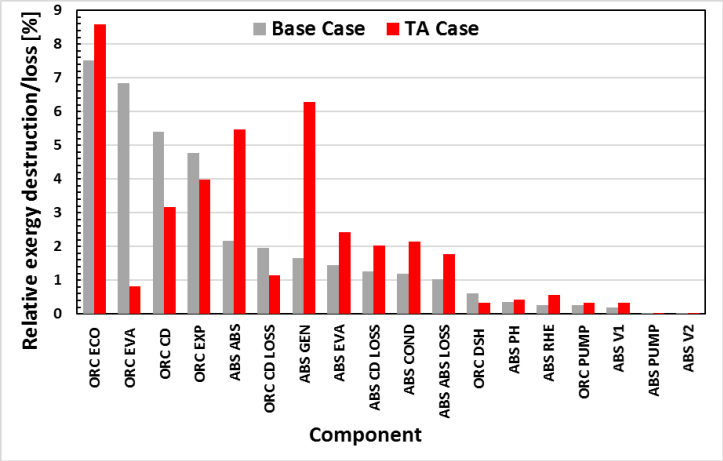

Figure 9: Relative component exergy destructions/losses.

The results in terms of component relative exergy destructions and losses for the TA Case are also collected, as reported in Figure 9. Differently from the Base Case, the highest exergy destructions occur in the ORC economizer (8.6%), in the ABS generator (6.3%) and absorber (5.5%). The generator temperature increase of 8°C is reflected in a higher temperature value at Point 18 (85°C instead of 77°C). This leads to a significant increase in the exergy destruction for the ABS generator (more than 300%). The relative exergy destruction of the ABS absorber is 60% greater than for the Base Case.

The brine reinjection loss is not shown in Figure 9, as its value (48.1%) is large for the TA case as well. The regulation constraints impose to reinject at this temperature level (T_3 = 83.8 °C) so that a variation in T_3 is not considered in terms of optimization. Considering the brine reinjection loss, the exergy efficiency (Eqs. 23 or 24) is equal to η_{x2}= 0.277; if the reinjection loss were neglected ($\dot{E}x_{t_{in}} = \left(\dot{E}x_{t_1} - \dot{E}x_{t_3}\right)$) the exergy efficiency would rise to η_{x1}= 0.410. The exergy efficiency of the TA case (27.7%) is decreased by about 3 points percentage compared to the one of the Base Case (30.8%). One way to explain the increase of the

irreversibility and the decrement of the exergy efficiency is to study the temperature profiles of the heat exchangers in the system [51]. On the one hand, the log mean temperature difference (LMTD) at the ABS generator increases from 8.44°C (Base Case) to 19.63°C (TA Case), thus the heat is exchanged with higher irreversibility. On the other hand, in the ORC the heat is exchanged with lower irreversibility, because the LMTD at the economizer varies from 25.28°C (Base Case) to 25.01°C (TA Case), while the LMTD at the evaporator undergoes a significant decrease, from 18.2°C (Base Case) to 8.43°C (TA Case). As the increment in the LTMD at the ABS generator is greater than the decrement at the ORC evaporator, the overall effect is that the exergy efficiency of the TA Case slightly decreases.

5 Conclusions

Two case studies were presented and discussed for the cold and power system using different low-temperature geothermal resources, which are generally much more widespread worldwide compared to conventional high-temperature ones.

Energy and exergy analyses of a cascade system configuration of an ORC coupled to an absorption cycle have been performed.

To identify the main sources of irreversibility and to determine the performance of the system, a detailed thermodynamic modeling of the proposed system has been developed and verified.

The Base Case showed a EUF of 28.1% and an exergy efficiency of 30.8%, neglecting the brine reinjection loss. The highest exergy destructions are in the ORC economizer (7.6%) and in the ORC evaporator (6.9%), while the ABS components have relatively low exergy destructions (below 2%). The high exergy destruction at the ORC evaporator for the Base Case is due to the poor matching of the heat transfer profile of the geothermal fluid resource, which determines a large heat transfer exergy destruction.

Regarding the Torre Alfina Case, the parametric analyses screened the performance and examined the effect of the high pressure of the ORC over the pinch point temperature difference and the surfaces of heat exchangers. The variation of the ORC working fluid flow rate can be used to trim the purpose of the plant to local requirements.

The distribution of exergy destructions and losses is affected by the different resource conditions: the highest exergy destructions are in the ORC economizer (8.6%), the ABS generator (6.3%) and in the ABS absorber (5.4%), and represent overall more than 20% of the total exergy input from the geo-fluid. Under optimized conditions, the TA Case (targeted on a 5 MW power output) showed an EUF of 46.2% and an exergy efficiency of 27.7%, neglecting the brine reinjection loss.

The results show that the exergy efficiency is decreased by 3.1 percentage point compared to the Base Case, but the EUF is increased by 18.1 percentage points.

Thus, the better resource conditions drive the design optimization to the production of power rather than cold; consequently, the relative exergy destructions in the ORC section are reduced; on the other hand, the performance of the ABS section becomes relevant for the exergy balance. From the exergetic point of view, the resource of TA cannot be exploited in the same efficient way as the Base Case, due to the limitation of the maximum net power to 5 MW and the irreversibilities associated to the heat transfer in the ABS evaporator. However, the better resource conditions allow a higher production of power and cold, which are suitable for industrial and commercial applications.

Nomenclature:

List of symbols

HE Heat exchanger

GEN Generator

PH Preheater

CD Condenser

AB Absorber

EVA Evaporator

ORC Organic Rankine cycle

V Throttling valve

A Surface of heat exchanger, m^2

COP Coefficient of performance, (-)

EUF Energy utilization factor, (-)

ex Exergy, kJ/kg

Ex_t Total exergy, kW

h Enthalpy, kJ/kg

$\dot{m}$ Mass flow rate, kg/s

p Pressure, kPa

$\dot{W}$ Power, W

$\dot{Q}$ Heat rate, kW

s Entropy, kJ/(kg K)

T Temperature, °C

DTU Temperature difference, °C

q Quality, (-)

x Concentration of LiBr, (-)

LMTD Log mean temperature difference, (-)

U Overall heat transfer coefficient, $W/(m^2 K)$

Greek letter

ΔT Temperature difference

ε Effectiveness

η Efficiency

Subscripts

0 Reference state

1,2,.. Point indicator

a Approach

AB Absorber

ABS Absorption chiller

C Cold side

CD Condenser

CW Cooling water

D Destruction

ECO Economizer

env To the environment

EVA Evaporator

EXP	Expander
H	Hot side
GB	Geothermal Brine
in	Input
L	Loss
ORC	Organic Rankine cycle
OUTs	Outputs
pp	Pinch Point
s	Isentropic (ideal)
x1	Exergy 1
x2	Exergy 2 (including reinjection loss)

References

[1] Adams S, Klobodu EKM, Apio A. Renewable and non-renewable energy, regime type and economic growth. Renew Energy 2018;125:755–67. doi:10.1016/j.renene.2018.02.135.

[2] Cozzolino R, Tribioli L, Bella G. Power management of a hybrid renewable system for artificial islands: A case study. Energy 2016;106:774–89. doi:10.1016/J.ENERGY.2015.12.118.

[3] Tribioli L, Cozzolino R. Techno-economic analysis of a stand-alone microgrid for a commercial building in eight different climate zones. Energy Convers Manag 2019;179:58–71. doi:10.1016/J.ENCONMAN.2018.10.061.

[4] Jurasz J, Mikulik J, Krzywda M, Ciapała B, Janowski M. Integrating a wind- and solar-powered hybrid to the power system by coupling it with a hydroelectric power station with pumping installation. Energy 2018;144:549–63. doi:10.1016/j.energy.2017.12.011.

[5] Moya D, Aldás C, Kaparaju P. Geothermal energy: Power plant technology and direct heat applications. Renew Sustain Energy Rev 2018;94:889–901. doi:10.1016/J.RSER.2018.06.047.

[6] Templeton JD, Ghoreishi-Madiseh SA, Hassani F, Al-Khawaja MJ. Abandoned petroleum wells as sustainable sources of geothermal energy. Energy 2014;70:366–73. doi:10.1016/J.ENERGY.2014.04.006.

[7] Shortall R, Davidsdottir B, Axelsson G. Geothermal energy for sustainable development: A review of sustainability impacts and assessment frameworks. Renew Sustain Energy Rev 2015;44:391–406. doi:10.1016/J.RSER.2014.12.020.

[8] Yildirim D, Ozgener L. Thermodynamics and exergoeconomic analysis of geothermal power plants. Renew Sustain Energy Rev 2012;16:6438–54. doi:10.1016/J.RSER.2012.07.024.

[9] Budisulistyo D, Krumdieck S. Thermodynamic and economic analysis for the pre-feasibility study of a binary geothermal power plant. Energy Convers Manag 2015;103:639–49. doi:10.1016/J.ENCONMAN.2015.06.069.

[10] DiPippo R. Geothermal power plants: Evolution and performance assessments. Geothermics 2015;53:291–307. doi:10.1016/j.geothermics.2014.07.005.

[11] Van Erdeweghe S, Van Bael J, Laenen B, D'haeseleer W. Optimal combined heat-and-

power plant for a low-temperature geothermal source. Energy 2018;150:396–409. doi:10.1016/J.ENERGY.2018.01.136.

[12] Imran M, Usman M, Park B-S, Yang Y. Comparative assessment of Organic Rankine Cycle integration for low temperature geothermal heat source applications. Energy 2016;102:473–90. doi:10.1016/J.ENERGY.2016.02.119.

[13] Van Erdeweghe S, Van Bael J, Laenen B, D'haeseleer W. Feasibility study of a low-temperature geothermal power plant for multiple economic scenarios. Energy 2018;155:1004–12. doi:10.1016/J.ENERGY.2018.05.028.

[14] Walraven D, Laenen B, D'haeseleer W. Economic system optimization of air-cooled organic Rankine cycles powered by low-temperature geothermal heat sources. Energy 2015;80:104–13. doi:10.1016/J.ENERGY.2014.11.048.

[15] Zeyghami M. Performance analysis and binary working fluid selection of combined flash-binary geothermal cycle. Energy 2015;88:765–74. doi:10.1016/J.ENERGY.2015.05.092.

[16] Liu Q, Duan Y, Yang Z. Performance analyses of geothermal organic Rankine cycles with selected hydrocarbon working fluids. Energy 2013;63:123–32. doi:10.1016/J.ENERGY.2013.10.035.

[17] Zhai H, Shi L, An Q. Influence of working fluid properties on system performance and screen evaluation indicators for geothermal ORC (organic Rankine cycle) system. Energy 2014;74:2–11. doi:10.1016/J.ENERGY.2013.12.030.

[18] Liu Q, Duan Y, Yang Z. Effect of condensation temperature glide on the performance of organic Rankine cycles with zeotropic mixture working fluids. Appl Energy 2014;115:394–404. doi:10.1016/J.APENERGY.2013.11.036.

[19] Cho H, Smith AD, Mago P. Combined cooling, heating and power: A review of performance improvement and optimization. Appl Energy 2014;136:168–85. doi:10.1016/J.APENERGY.2014.08.107.

[20] Cozzolino R. Thermodynamic Performance Assessment of a Novel Micro-CCHP System Based on a Low Temperature PEMFC Power Unit and a Half-Effect Li/Br Absorption Chiller. Energies 2018;11:1–21.

[21] Tempesti D, Manfrida G, Fiaschi D. Thermodynamic analysis of two micro CHP systems operating with geothermal and solar energy. Appl Energy 2012;97:609–17.

doi:10.1016/j.apenergy.2012.02.012.

[22] Lozano MA, Carvalho M, Serra LM. Operational strategy and marginal costs in simple trigeneration systems. Energy 2009;34:2001–8. doi:10.1016/J.ENERGY.2009.08.015.

[23] Loreti G, Facci AL, Baffo I, Ubertini S. Combined heat, cooling, and power systems based on half effect absorption chillers and polymer electrolyte membrane fuel cells. Appl Energy 2019;235:747–60. doi:10.1016/J.APENERGY.2018.10.109.

[24] Zare V. A comparative thermodynamic analysis of two tri-generation systems utilizing low-grade geothermal energy. Energy Convers Manag 2016;118:264–74. doi:10.1016/j.enconman.2016.04.011.

[25] Fiaschi D, Lifshitz A, Manfrida G, Tempesti D. An innovative ORC power plant layout for heat and power generation from medium- to low-temperature geothermal resources. Energy Convers Manag 2014;88:883–93. doi:10.1016/j.enconman.2014.08.058.

[26] Goswami DY, Xu F. Analysis of a New Combined Power and Cooling 1999;121:91–7.

[27] Fiaschi D, Manfrida G, Talluri L. Water-Ammonia Cycles for the Utilization of Low Temperature Geothermal Resources. ASME 2015 Power Conf., ASME; 2015, p. V001T01A014. doi:10.1115/POWER2015-49531.

[28] Islam S, Dincer I. Development, analysis and performance assessment of a combined solar and geothermal energy-based integrated system for multigeneration. Sol Energy 2017;147:328–43. doi:10.1016/J.SOLENER.2017.02.048.

[29] Zhao Y, Wang J, Cao L, Wang Y. Comprehensive analysis and parametric optimization of a CCP (combined cooling and power) system driven by geothermal source. Energy 2016;97:470–87. doi:10.1016/J.ENERGY.2016.01.003.

[30] Akbari Kordlar M, Mahmoudi SMS. Exergeoconomic analysis and optimization of a novel cogeneration system producing power and refrigeration. Energy Convers Manag 2017;134:208–20. doi:10.1016/J.ENCONMAN.2016.12.007.

[31] Ufficio Nazionale Minerario per gli Idrocarburi e la Geotermia n.d. http://unmig.sviluppoeconomico.gov.it/unmig/geotermia (accessed December 25, 2018).

[32] Rahbar K, Mahmoud S, Al-Dadah RK, Moazami N. Parametric analysis and optimization of a small-scale radial turbine for Organic Rankine Cycle. Energy 2015;83:696–711. doi:10.1016/J.ENERGY.2015.02.079.

[33] Chen H, Goswami DY, Stefanakos EK. A review of thermodynamic cycles and working fluids for the conversion of low-grade heat. Renew Sustain Energy Rev 2010;14:3059–67. doi:10.1016/j.rser.2010.07.006.

[34] Liu X, Wang X, Zhang C. Sensitivity analysis of system parameters on the performance of the Organic Rankine Cycle system for binary-cycle geothermal power plants. Appl Therm Eng 2014;71:175–83. doi:10.1016/J.APPLTHERMALENG.2014.06.048.

[35] Franco A, Villani M. Optimal design of binary cycle power plants for water-dominated, medium-temperature geothermal fields. Geothermics 2009;38:379–91. doi:10.1016/J.GEOTHERMICS.2009.08.001.

[36] Horuz I. A comparison between ammonia-water and water-lithium bromide solutions in vapor absorption refrigeration systems. Int Commun Heat Mass Transf 1998;25:711–21. doi:10.1016/S0735-1933(98)00058-X.

[37] Herold KE, Radermacher R, Klein SA. Absorption chillers and heat pumps. n.d.

[38] Szargut J, Morris DR, Steward FR. Exergy analysis of thermal, chemical, and metallurgical processes. Hemisphere; 1988.

[39] Kotas TJ. The exergy method of thermal plant analysis. Butterworths; 1985.

[40] Ministero dello sviluppo economico - DGS-UNMIG n.d. http://unmig.mise.gov.it/unmig/geotermia/pozzi/pozzi.asp (accessed February 14, 2018).

[41] Impianto pilota geotermico denominato “Torre Alfina”; nel comune di Acquapendente (VT) - Info - Valutazioni Ambientali - VAS - VIA n.d. http://www.va.minambiente.it/it-IT/Oggetti/Info/1566 (accessed February 14, 2018).

[42] Buonasorte G, Cataldi R, Ceccarelli A, Costantini A, D’Offizi S, Lazzarotto A. Ricerca ed esplorazione nell’area geotermica di Torre Alfina (Lazio-Umbria). BollSocGeolIt 1988:265–337.

[43] Buonasorte G, Cataldi R, Pandeli E, Fiordalisi A. The Alfina 15 well: Deep Geological data from Northern Latium (Torre Alfina Geothermal area) 1991.

[44] EES: Engineering Equation Solver | F-Chart Software : Engineering Software n.d. http://www.fchart.com/ees/ (accessed December 25, 2018).

[45] Sun J, Liu Q, Duan Y. Effects of evaporator pinch point temperature difference on thermo-economic performance of geothermal organic Rankine cycle systems.

Geothermics 2018;75:249–58. doi:10.1016/J.GEOTHERMICS.2018.06.001.

[46] Heberle F, Brüggemann D, Heberle F, Brüggemann D. Thermo-Economic Evaluation of Organic Rankine Cycles for Geothermal Power Generation Using Zeotropic Mixtures. Energies 2015;8:2097–124. doi:10.3390/en8032097.

[47] Albers J, Nurzia G, Ziegler F. Simulation and Experimental Analysis of a Solar Driven Absorption Chiller With Partially Wetted Evaporator. ASME 2008 2nd Int. Conf. Energy Sustain. Vol. 2, ASME; 2008, p. 561–8. doi:10.1115/ES2008-54102.

[48] Goswami DY, Hingorani S, Mines G. A Laser-Based Technique for Particle Sizing to Study Two-Phase Expansion in Turbines. J Sol Energy Eng 1991;113:211. doi:10.1115/1.2930495.

[49] Gyarmathy G. Nucleation of steam in high-pressure nozzle experiments. Proc Inst Mech Eng Part A J Power Energy 2005;219:511–21. doi:10.1243/095765005X31388.

[50] Besarati SM, Yogi Goswami D. Analysis of Advanced Supercritical Carbon Dioxide Power Cycles With a Bottoming Cycle for Concentrating Solar Power Applications. J Sol Energy Eng 2013;136:010904. doi:10.1115/1.4025700.

[51] Mines G. Binary geothermal energy conversion systems: Basic Rankine, dual–pressure, and dual–fluid cycles. Geotherm Power Gener 2016:353–89. doi:10.1016/B978-0-08-100337-4.00013-9.